6-22-2023

GABAergic synaptic scaling is triggered by changes in spiking activity rather than transmitter receptor activation

Carlos Gonzalez-Islas

Zahraa Sabra

Ming-fai Fong

Pernille Bülow

Nicholas Au Yong

See next page for additional authors

GABAergic synaptic scaling is triggered by changes in spiking activity rather than transmitter receptor activation.

Carlos Gonzalez-Islas[1,2], Zahraa Sabra[4], Ming-fai Fong[1,3], Pernille Bülow[1], Nicholas Au Yong[4], Kathrin Engisch[5], and *Peter Wenner[1].

1. Department of Cell Biology. Emory University, School of Medicine, Atlanta, GA, 30322.
2. Doctorado en Ciencias Biológicas Universidad Autónoma de Tlaxcala, Tlax. México
3. Department of Biomedical Engineering, Georgia Tech and Emory University, Atlanta, GA
4. Department of Neurosurgery, Emory University, Atlanta, GA, 30322
5. Department of Neuroscience, Cell Biology and Physiology, Wright State University, Dayton, OH 45435

ORCID iDs:
C.G. - 0000-0002-3785-4494, Z.S. - 0000-0002-2343-7286, M.F. - 0000-0002-2336-4531, P.B. - 0000-0003-1884-6189, N.A.Y. - 0000-0002-7898-7832, K.E. - 0000-0002-1058-5343, P.W. - 0000-0002-7072-2194

*Peter Wenner – corresponding author
Emory University, School of Medicine
Department of Cell Biology,
615 Michael St., Rm 601
Atlanta, GA, 30322
pwenner@emory.edu
ph. 404 727-1517

Author Contributions:

C.G. and P.W. designed research; C.G, P.B., and M.F. performed research; C.G, Z.S., M.F., N.A.Y., K.E. and P.W. analyzed data; C.G., M.F., K.E. and P.W. wrote the paper.

Competing Interest Statement: We have no competing interests.

Keywords: Homeostatic, Plasticity, Scaling, Optogenetic, GABA

This PDF file includes:

Main Text
Figures 1 to 6, and Supplemental Figures 1-4

Abstract

Homeostatic plasticity represents a set of mechanisms that are thought to recover some aspect of neural function. One such mechanism called AMPAergic scaling was thought to be a likely candidate to homeostatically control spiking activity. However, recent findings have forced us to reconsider this idea as several studies suggest AMPAergic scaling is not directly triggered by changes in spiking. Moreover, studies examining homeostatic perturbations *in vivo* have suggested that GABAergic synapses may be more critical in terms of spiking homeostasis. Here we show results that GABAergic scaling can act to homeostatically control spiking levels. We find that increased or decreased spiking in cortical cultures triggers multiplicative GABAergic upscaling and downscaling, respectively. In contrast, we find that changes in AMPAR or GABAR transmission only influence GABAergic scaling through their indirect effect on spiking. We propose that GABAergic scaling, rather than glutamatergic scaling, is a key player in spike rate homeostasis.

Significance Statement

The nervous system maintains excitability in order to perform network behaviors when called upon to do so. Networks are thought to maintain spiking levels through homeostatic synaptic scaling, where compensatory multiplicative changes in synaptic strength are observed following alterations in cellular spike rate. Although we demonstrated that AMPAergic synaptic scaling does not appear meet these criteria as a spike rate homeostat, we now show that GABAergic scaling does. Here we present evidence that the characteristics of GABAergic scaling place it in an excellent position to be a spiking

homeostat. This work highlights the importance of inhibitory circuitry in the homeostatic control of excitability. Further, it provides a point of focus into neurodevelopmental disorders where excitability is impaired.

Introduction

Homeostatic plasticity represents a set of compensatory mechanisms that are thought to be engaged by the nervous system in response to cellular or network perturbations, particularly in developing systems (1). It has been postulated that synaptic scaling is one such mechanism where homeostatic compensations in the strength of the synapses onto a neuron occur following chronic perturbations in spiking activity or neurotransmitter receptor activation (neurotransmission)(2). Scaling is typically identified by comparing the distribution of miniature postsynaptic current (mPSC) amplitudes in control and activity-perturbed conditions. For instance, when spiking activity in cortical cultures was reduced for 2 days with the Na^+ channel blocker TTX or the AMPA/kainate glutamate receptor antagonist CNQX, the overall distribution of mEPSC amplitudes were increased (2). When first discovered, homeostatic synaptic scaling was thought to be triggered by the cell sensing its reduction in spike rate through associated calcium signaling. This was then believed to trigger a signaling cascade that increased AMPA receptor (AMPAR) insertion in a cell-wide manner such that all synapses increased synaptic strength multiplicatively based on each synapse's initial strength (3). This led to the idea that the scaling was a global phenomenon. In this way excitatory synaptic strength was increased across all of the cell's inputs in order to recover spiking activity without altering relative synaptic strengths resulting from Hebbian plasticity mechanisms. These

47 criteria, sensing spike rate and adjusting synaptic strengths multiplicatively, thus establish
48 the expectations of a spiking homeostat.

49 More recent work has demonstrated that AMPAergic synaptic scaling is more
50 complicated than originally thought. First, studies have now shown that increases in
51 mEPSC amplitudes or synaptic glutamate receptors often do not follow a simple
52 multiplicative function (4, 5). Rather, these studies show that changes in synaptic strength
53 at different synapses exhibit different scaling factors, arguing against a single
54 multiplicative scaling factor that alters synaptic strength globally across the cell. Second,
55 AMPAergic scaling triggered by receptor blockade induces a synapse-specific plasticity
56 rather than a cell-wide plasticity. Compensatory changes in synaptic strength were
57 observed in several studies where neurotransmission at individual synapses was reduced
58 (6-9). This synapse-specific plasticity would appear to be cell-wide if neurotransmission at
59 all synapses were reduced as occurs in the typical pharmacological blockades that are
60 used to trigger scaling. Regardless, this would still be a synapse specific plasticity,
61 determined at the synapse, rather than the cell sensing it's lowered spiking activity. Finally,
62 several different studies now suggest that reducing spiking levels in neurons is not
63 sufficient to trigger AMPAergic upscaling (however see (10)). Forced expression of a
64 hyperpolarizing conductance reduced spiking of individual cells but did not trigger scaling
65 (11). Further, optogenetic restoration of culture-wide spiking in the presence of AMPAergic
66 transmission blockade triggered AMPAergic scaling that was indistinguishable from that
67 of cultures where AMPAR block reduced spiking (no optogenetic restoration of spiking)
68 (12). Most studies that separate the importance of cellular spiking from synapse-specific
69 transmission suggest that AMPAergic scaling is triggered by changes in
70 neurotransmission, rather than a cell's spiking activity (9, 11-13). If AMPAergic scaling

71 does not act to homeostatically maintain spiking activity, then what homeostatic
72 mechanisms do?

73 Here, we consider the possibility that GABAergic, rather than glutamatergic,
74 synaptic scaling plays a role of spiking homeostat. Homeostatic regulation of GABAergic
75 miniature postsynaptic current (mIPSC) amplitude was first shown in excitatory neurons
76 following network activity perturbations (14). Similar to AMPAergic scaling, chronic
77 perturbations in AMPAR or spiking activity triggered mIPSC scaling through compensatory
78 changes in the number of synaptic $GABA_A$ receptors (14-18). However, the sensing
79 machinery for triggering GABAergic scaling appears to be distinct from that of AMPAergic
80 scaling (19). Further, GABAergic plasticity does appear to be a key player in the
81 homeostatic response *in vivo*, as many different studies have shown strong GABAergic
82 compensations following somatosensory, visual, and auditory deprivations (20-24). In
83 addition, these homeostatic GABAergic responses precede and can outlast compensatory
84 changes in the glutamatergic system. Here we describe that GABAergic scaling is
85 triggered by changes in spiking levels rather than changes in neurotransmission, that
86 GABAergic scaling is expressed in a multiplicative manner, and could contribute to the
87 homeostatic recovery of spiking activity. Our results suggest that GABAergic scaling
88 serves as a homeostat for spiking activity.

89

90 ## Results

91

92 **TTX and AMPAR blockade triggered a non-uniform scaling of AMPA mPSCs.**

93 Previously we have shown that blocking spike activity in neuronal cultures
94 triggered scaling in a non-uniform or divergent manner, such that different synapses

scaled with different scaling ratios (4, 25). Importantly, these results were consistent across independent studies performed in three different labs using rat or mouse cortical cultures, or mouse hippocampal cultures. We quantitatively evaluated scaling by dividing the rank-ordered mEPSC amplitudes following treatment with TTX by the rank-ordered mEPSC amplitudes from the control cultures and plotted these ratios for all such comparisons. Previously, scaling had been thought to be multiplicative, meaning all mPSC amplitudes were altered by a single multiplicative factor. If true for AMPAergic scaling, then our ratio plots should have produced a horizontal line at the scaling ratio. However, we found that ratios progressively increased across at least 75% of the distribution of amplitude ratios. Still, it was unclear whether this was true for all forms of AMPAergic scaling triggered by different forms of activity blockade. Therefore, we repeated this analysis on the data from our previous study (12), but now on AMPAergic scaling produced by blocking AMPAR neurotransmission (CNQX), rather than TTX. We found that the scaling was non-uniform and replicated the scaling triggered by TTX application where there was a progressive increase in scaling ratios from 1.2 to 1.5 across the distribution of ratios (Supplemental Figure 1). The results suggest that AMPAergic scaling produced by blocking glutamatergic transmission or spiking in culture was not multiplicative, but rather different synapses increased by different scaling factors.

TTX and AMPAR blockade reduced both spiking and GABAergic mIPSC amplitude.

Previously we made the surprising discovery that AMPAergic upscaling in rat cortical cultures was triggered by a reduction in AMPAR activation rather than a reduction in spiking activity (12). Here we tested whether GABAergic scaling was dependent on AMPAR activation or rather might be mediated by changes in spiking activity levels. We plated E18 mouse cortical neurons on 64 channel planar multi-electrode arrays (MEAs)

and allowed the networks to develop for ~14 days *in vitro* (DIV), a time point where most cultures develop a network bursting behavior (Supplemental Figure 2) (26). We used a custom written Matlab program that was able to detect and compute overall spike rate and burst frequency (Supplemental Figure 2, see methods). We again found that TTX abolished bursts and spiking activity (n=2, Supplemental Figure 3). On the other hand, AMPAR blockade (20μM) merely reduced bursts and spiking, with a greater effect on bursting. An example of the influence of adding 20 μM CNQX to the culture is shown in Figure 1A. Similar to our findings in rat cortical cultures (12), CNQX dramatically reduced burst frequency and maintained this reduction for the entire 24hrs of treatment (Figure 1B). Overall spike frequency was also reduced in the first 6 hours, but then recovered over the 24 hour drug treatment (Figure 1C). While overall spiking was recovered, we did note that this was highly variable.

In order to examine the possibility that compensatory changes in GABAergic synaptic strength could have contributed to the recovery of the network spiking activity we assessed synaptic scaling by measuring mIPSC amplitudes in pyramidal-like neurons in a separate set of cortical cultures plated on coverslips. We found that both activity blockade with TTX and AMPAergic blockade with CNQX triggered a dramatic compensatory reduction in mIPSC amplitude compared to control (untreated) cultures (Figure 2A). Even though TTX completely abolished spiking while CNQX only reduced spiking, both treatments triggered a similar reduction in average mIPSC amplitude. In order to more carefully compare the GABAergic scaling that is triggered by TTX and CNQX mechanistically, we created scaling ratio plots as described above (4). In addition to identifying the multiplicative nature of this form of plasticity, it provides a means to mechanistically assess distinct forms of scaling that are triggered in different ways (TTX

vs CNQX). In Figure 2B we show that TTX-induced scaling does produce a largely multiplicative downscaling with a scaling factor of slightly less than 0.5. GABAergic scaling induced by CNQX-treatment produced a similar ratio plot that only differed in that it had a slightly higher ratio through the middle of the plot (Figure 2B). This is consistent with the idea that the mechanisms were similar, although TTX-induced scaling may be slightly more effective through much of the distribution, possibly related to the fact that TTX completely abolished spiking in these cultures. These results are consistent with the idea that either spiking or reduced AMPA receptor activation could trigger the GABAergic downscaling since both would be reduced by TTX or CNQX.

Optogenetic restoration of spiking in the presence of AMPAR blockade prevented GABAergic downscaling.

In order to separate the importance of spiking levels from AMPAR activation in triggering GABAergic downscaling we blocked AMPARs while restoring spike frequency as we had done in a previous study assessing AMPAergic scaling (12). Cultures were plated on the MEA and infected with ChR2 under the human synapsin promoter on DIV 1. Experiments were carried out on ~ DIV14, when cultures typically express network bursting. Baseline levels of spike frequency were measured in a 3-hour period before the addition of 20μM CNQX (Figure 3A). We then used a custom written TDT Synpase software that activated a blue light photodiode to initiate bursts (see methods) whenever the running average of the firing rate fell below the baseline level, established before the addition of the drug. In this way we could optically induce bursts of normal structure and largely restore spike rate to pre-drug values in the cultues while blocking AMPAR activation (Figure 3B).

We have already established that bursts and spiking were reduced following the application of CNQX (Figure 1). However, when we optogenetically activated the cultures in the presence of CNQX we found that both the burst rate and spike frequency were increased compared to CNQX treatment alone, no optostimualtion (Supplemental Figure 4). Because the program was designed to maintain total spike frequency, photostimulation of CNQX-treated cultures did a relatively good job at recovering this parameter to control levels (Figure 3D). In fact, spike frequency was slightly, but not significantly, above control levels through the 24 hour recording period (Figure 3D). On the other hand, optostimulation in CNQX did not completely return burst frequency back to control levels (Figure 3C).

We next assessed mIPSC amplitudes using whole cell recordings taken from cultures plated on MEAs. After blocking AMPAR activation without optogenetic restoration of spiking activity, we found that mIPSC amplitudes were significantly reduced compared to control conditions (Figure 4A), as we had shown for CNQX treatment on cultures plated on coverslips (Figure 2A). Strikingly, when spiking activity was optogentically restored in the presence of CNQX for 24 hours we observed that mIPSCs were no different than control values (same as control, larger than CNQX only – Figure 4A). This result suggested that unlike AMPAergic upscaling, GABAergic downscaling was dependent on spiking activity levels. In order to compare scaling profiles we plotted the scaling ratios for these different treatments. Not surprisingly, we found that MEA-plated cultures treated with CNQX but given no optogenetic stimulation were similar to CNQX-treated cultures plated on coverslips (CNQX/control ~ 0.5, Figure 4B vs Figure 2B). Ratio plots of cultures treated with CNQX where activity was restored optogenetically compared to controls demonstrated a fairly linear relationship with a ratio of around 1 through most of the

distribution suggesting the mIPSCs in these two conditions were similar and therefore unscaled (Figure 4B). Interestingly, the scaling ratio and the average mIPSC amplitudes in the optogenetically activated cultures were slightly larger than control mIPSCs which may be due to the slight increase in spiking in optogeneticallly stimulated cultures. Together, these results are consistent with the idea that GABAergic downscaling was triggered by reductions in spiking activity, not AMPA receptor activation, and was multiplicative and therefore satisfied the criterion for being a spiking homeostat.

Enhancement of AMPAR currents triggered GABAergic upscaling though spiking activity, not receptor activation.

While reductions in spiking activity triggered a GABAergic downscaling, it was not clear whether increases in spiking activity could trigger compensatory GABAergic upscaling. To test for such a possibility, we exposed the cultures to cyclothiazide (CTZ), an allosteric enhancer of AMPA receptors that also enhances spontaneous currents (12). Due to the hydrophobic nature of CTZ it was necessary to dissolve it in ethanol, and used ethanol without CTZ as a control (final solution 1:1000 ethanol). In addition to increasing AMPAR activation, CTZ application trended to increase overall spiking activity and burst rate in our MEA-plated cultures during the 24 hour application, although this was quite variable and only the 3 hour timepoint for spike frequency reached significance (Figure 5A-B). We then treated coverslip-plated cultures with CTZ for 24 hours and measured GABAergic mIPSC amplitude and found that this did indeed produce a compensatory increase in GABA mIPSC amplitude (Figure 5C). In our previous study we found that CTZ reduced TTX-induced AMPAergic upscaling suggesting that AMPAR activation, independent of spiking, could influence scaling (12). To test whether this CTZ-mediated increase in GABAergic mIPSC amplitude was dependent on spiking activity we treated

cultures with the combination of CTZ and TTX for 24 hrs. Here we found that the CTZ-induced increase in mIPSC amplitude was converted to a reduction in amplitudes that was no different than TTX treatment alone (Figure 5D). The finding that GABAergic mIPSC amplitudes were scaled in opposite directions depending on whether we treated with CTZ or CTZ + TTX suggested that enhancing AMPAR activation had no direct influence on GABAergic scaling, but rather it was CTZ's ability to increase spiking that triggered the scaling. To determine if these changes in mIPSC amplitude were of a multiplicative scaling nature we made ratio plots. This demonstrated that both CTZ increases and CTZ+TTX decreases in mIPSC amplitude were multiplicative and therefore represented scaling (Figure 5E, CTZ – scaling ratio of 1.5, CTZ+TTX - scaling ratio of 0.6). Further, the scaling ratio plot for CTZ + TTX looked similar to those of TTX alone (compare Figure 5E and 2B). These results showed a compensatory upward and downward GABAergic scaling and both were dependent on spiking activity levels rather than AMPAergic receptor activation. This is therefore distinct from upward AMPAergic scaling, which is dependent on glutamatergic receptor activation.

Blocking GABAergic receptors for 24 hours triggered upscaling of GABAergic mIPSCs.

The above results suggested that GABAergic scaling was dependent on the levels of spiking activity. However, one alternative possibility was that these changes in GABA mPSCs were due to changes in GABAergic receptor activation. It is unlikely that alterations in GABAR activation trigger compensations at the receptor level (e.g. reduced GABAR activity increases synaptic GABARs – upscaling), as CNQX treatment would decrease GABAR activation but results in a GABAergic downscaling, and CTZ should increase GABAR activation but results in a GABAergic upscaling. On the other hand,

GABA receptor activation could act as a proxy for activity levels (e.g. increases in GABAR activation signal an increase in spiking activity and this triggers a compensatory GABAergic upscaling to recover activity levels). In this way, GABARs sense changes in spiking activity levels and directly trigger GABAergic scaling to recover activity. To address this possibility, we treated cultures with the $GABA_A$ receptor antagonist bicuculline to chronically block GABAergic receptor activation while increasing spiking activity. If increased spiking activity is directly the trigger (not mediated through GABAR activity), then we would expect to see GABAergic upscaling. On the other hand, if GABAR activation is a proxy for spiking then blockade of these receptors would indicate low activity levels and we would expect a downscaling to recover the apparent loss of spiking. GABAR block produced an upward trend in both burst frequency (Figure 6A) and spike frequency (Figure 6B). We measured mIPSCs in a separate cohort of cultures plated on coverslips which were treated with bicuculline for 24 hours, and we observed GABAergic upscaling (Figure 6C). These results suggested that direct changes in spiking activity, rather than AMPA or GABA receptor activation triggered compensatory GABAergic scaling. The scaling ratio plots were again relatively flat, with a scaling ratio of around 1.5 suggesting a multiplicative GABAergic upscaling (Figure 6D) that was similar to CTZ-induced upward scaling (Figure 5E).

Discussion

Here we find that GABAergic up- and downscaling exhibits all the features expected for a key homeostatic mechanism that maintains spike rate – 1) was triggered by alterations in spike rate, rather than neurotransmission, 2) was expressed multiplicatively, and 3) occurred by the time the spike rate had recovered. First, GABAergic

scaling was triggered by altered spiking levels. We found that CNQX-triggered GABAergic downscaling was abolished when we optogenetically restored spiking activity levels (Figure 3-4), that increasing spiking with bicuculline or CTZ both triggered GABAergic upscaling (Figures 5-6), and that CTZ-induced upscaling was converted to downscaling when we concurrently blocked spiking with TTX (Figure 5C-D). Further, the findings suggest that altering neurotransmission did not contribute to GABAergic scaling. Increasing AMPAergic transmission with CTZ in the presence of TTX had no impact on downscaling as it was no different than following TTX treatment alone (Figure 5D). Also, if GABA transmission were a proxy for activity levels, then blocking $GABA_A$ receptors would mimic activity blockade and should lead to a compensatory downscaling. However, bicuculline (reduced GABAR activity) and CTZ (increased GABAR activity), both increased spiking and triggered a GABAergic upscaling consistent with the idea that spiking was the critical feature (Figure 5-6). Second, a global change in GABA synaptic strength throughout the cell should be expressed as a single multiplicative scaling factor, which is largely what we saw (Figures 2, 4-6). Finally, if scaling contributed to a homeostatic recovery of activity, then GABAergic scaling should have been expressed by the time the network had fully recovered its spiking levels and it did (Figures 1 & 2). Although AMPAergic scaling was initially thought to play the role of spiking homeostat, it appears more likely that GABAergic scaling is playing this role.

In the original study describing AMPAergic synaptic scaling, the authors triggered this plasticity by blocking spiking activity with TTX or blocking AMPAergic neurotransmission with CNQX (2). Similar results have now been demonstrated in multiple tissues and labs (25). It was thought that AMPAergic scaling was a homeostatic mechanism, triggered by alterations in spiking and likely calcium transients associated

with a cellular spiking; once the cell drifted outside the setpoint for spiking a cell-wide signal was activated that changed the synaptic strengths of all AMPAergic inputs by a single multiplicative scaling factor to return the cell to the spiking set point (3). In this way, AMPAergic scaling could homeostatically regulate spiking levels, while also preserving the relative differences in synaptic strength set up by Hebbian plasticity mechanisms. However, the triggers and multiplicative nature of the scaling appear to be more complex than our original understanding. Altering spiking levels in individual cells in some studies triggers scaling (10, 27), but not in other studies (11, 28). Further, the multiplicative nature of scaling following TTX treatment does not fit our recent work showing different synapses have different scaling factors (4) and this is consistent with another study that followed AMPAR expression following TTX + APV treatment (5). In the current study we show that AMPAergic scaling triggered by AMPAR blockade also produced a non-uniform scaling (Supplemental Figure 1). In addition, several studies have suggested that glutamate receptor activation due to action potential-independent spontaneous release could play a significant role in triggering AMPAergic scaling (7, 12, 29). In recent years it has become clear that when glutamatergic neurotransmission is reduced at individual synapses there is a synapse-specific compensatory increase in synaptic strength mediated by an insertion of AMPA receptors. Neurotransmission has been reduced by local application of a neurotransmitter antagonist (7), hyperpolarization of individual presynaptic inputs that are unlikely to alter the postsynaptic neuron's spiking (6, 8), or altering the activity of individual sensory pathways *in vivo* (9). These perturbations result in altered AMPA receptor trafficking, which strengthen only the synapses that were inhibited. When all AMPAergic synapses in the culture were blocked with CNQX it should be expected that all synapses would strengthen due to this neurotransmission-based compensatory plasticity. Because CNQX also reduced spiking levels, one might have expected that this reduced spiking

would add to the overall synaptic strengthening. However, as we have shown, putting back spiking activity levels and their associated calcium transients in the presence of CNQX had no effect on AMPAergic scaling (no reduction in the existing scaling (12)). This demonstrated that CNQX-triggered scaling was not dependent on reduced spiking. Because AMPAergic scaling does not act in a multiplicative manner and maintain relative differences in a cell's synaptic strengths and because it is not directly following spiking activity levels, it does not fulfill the expectations of a homeostat for spiking. Rather, AMPAergic scaling in many cases appears to act to homeostatically maintain the effectiveness of individual synapses.

Previously, in embryonic motoneurons we found that both GABAergic and AMPAergic scaling was mediated by changes in GABAR activation from spontaneous release rather than changes in spiking activity (13, 30). However, this was at a developmental stage when GABA was depolarizing and could potentially activate calcium signaling pathways. On the other hand, spike rate homeostasis through the GABAergic system is consistent with many previous studies in which sensory input deprivation *in vivo* led to rapid compensatory disinhibition (31, 32). For instance, one day of visual deprivation (lid suture) reduced evoked spiking in fast spiking parvalbumin (PV) interneurons and this was thought to underlie the recovery of pyramidal cell responses to visual input at this point (24). One day of whisker deprivation between P17 and P20 produced a reduction of PV interneuron firing that was due to reduced intrinsic excitability in the GABAergic PV neuron (20). In addition, one day after enucleation of the eye, the excitatory to inhibitory synaptic input ratio in pyramidal cells was dramatically increased due to large reductions in GABAergic inputs to the cell (23). This disinhibition occurs rapidly (22) and can outlast changes in glutamatergic counterparts (21, 23). These results highlight the important role

that inhibitory interneurons play in the homeostatic maintenance of spiking activity. Further, these cells have extensive connectivity with pyramidal cells, placing them in a strong position to influence network excitability (33, 34). Here we show a critical feature of homeostatic regulation of spiking is through one aspect of inhibitory control, GABAergic synaptic scaling.

It is not clear what specific features of spiking triggers GABAergic scaling. GABAergic scaling may require the reduction of spiking in multiple cells in a network, rather than a single cell. Reduced spiking with sporadic expression of a potassium channel in one hippocampal cell in culture did not induce GABAergic scaling in that cell (16). Such a result could be mediated by the release of some activity-dependent factor from a collection of neurons. BDNF is known to be released in an activity-dependent manner and has been shown to mediate GABAergic downward scaling following activity block previously in both hippocampal and cortical cultures and could mediate the process (15, 35). On the other hand, another study increased spiking in hippocampal cultures and showed that homeostatic increases in mIPSC amplitudes were dependent on the individual cells spiking activity (17). Finally, in order to determine the importance of overall spike frequency vs. burst frequency in triggering GABAergic scaling, additional experiments will be necessary, as both were reduced in the CNQX-treated network (Figure 1). Interestingly, our optogenetic restoration experiments found that downward scaling was completely abolished, and in fact mIPSC amplitudes were slightly increased compared to controls (Figure 4). Optogenetic stimulation did not fully restore burst frequency but did restore overall spiking, which is more consistent with the idea that downward scaling is due to reduced overall spike frequency, rather than reduced burst frequency. However, it is difficult to fully assess such parameters as our MEA recordings

of network spiking activity were subject to high levels of variability and our intracellular recordings were carried out on coverslips on a separate electrophysiology rig with whole cell capabilities. Whatever the specific features of spiking activity that trigger GABAergic scaling, our results strongly point to the idea that GABAergic scaling, rather than glutamatergic scaling, serves the critical role of a spiking homeostat, and highlights the fundamentally important homeostatic nature of GABAergic neurons.

Materials and Methods

Cell Culture. Brain cortices were obtained from C57BL/6J embryonic day 18 mice from BrainBits or harvested from late embryonic cortices. Neurons were obtained after cortical tissue was enzymatically dissociated with papain. Cell suspension was diluted to 2,500 live cells per ml and 35,000 cells were plated on glass coverslips or planar MEA coated with polylysine (Sigma, P-3143) and laminin. The cultures were maintained in Neurobasal medium supplemented with 2% B27 and 2mM GlutaMax. No antibiotics or antimycotics were used. Medium was changed completely after one day in vitro (1 DIV) and half of the volume was then changed every 7 days. Spiking activity was monitored starting ~10 DIV to determine if a bursting phenotype was expressed and continuous recordings were made between 14-20 DIV. Cultures were discarded after 20 DIV. All protocols followed the National Research Council's Guide on regulations for the Care and Use of Laboratory Animals and from the Animal Use and Care Committee from Emory University.

Whole cell recordings. Pyramidal-like cells were targeted based on their large size. Whole-cell voltage clamp recordings of GABA mPSCs were obtained using an AxoPatch

200B amplifier, controlled by pClamp 10.1 software, low pass filtered at 5 KHz on-line and digitized at 20 KHz. Tight seals (>2 GΩ) were obtained using thin-walled boro-silicate glass microelectrodes pulled to obtain resistances between 7 and 10 MΩ. The intracellular patch solution contained the following (in mM): CsCl 120, NaCl 5, HEPES 10, $MgSO_4$ 2, $CaCl_2$ 0.1, EGTA 0.5, ATP 3 and GTP 1.5. The pH was adjusted to 7.4 with KOH. Osmolarity of patch solution was between 280-300 mOsm. Artificial Cerebral-Spinal Fluid (ACSF) recording solution contained the following (in mM): NaCl 126, KCl 3, NaH2PO4 1, $CaCl_2$ 2, $MgCl_2$ 1, HEPES 10 and D-glucose 25. The pH was adjusted to 7.4 with NaOH. GABAergic mPSCs were isolated by adding to ACSF (in µM): TTX 1, CNQX 20 and APV 50. Membrane potential was held at -70 mV and recordings were performed at room temperature. Series resistance during recordings varied from 15 to 20 MΩ and were not compensated. Recordings were terminated whenever significant increases in series resistance (> 20%) occurred. Analysis of GABA mPSCs was performed blind to condition with MiniAnalysis software (Synaptosoft) using a threshold of 5 pA for mPSC amplitude (50 mPSCs were taken from each cell and their amplitudes were averaged and each dot in the scatterplots represent the average of a single cell). Ratio plots of mIPSCs were constructed by taking a constant total number of mIPSCs from control and drug-treated cultures (e.g. 15 control cells with 40 mIPSCs from each cell and 20 CNQX-treated cells with 30 mIPSCs from each cell, 600 mIPSCs per condition). Then the amplitudes of mIPSCs from each condition were rank ordered from smallest to largest and plotted as a ratio of the drug-treated amplitude divided by the control amplitude, as we have described previously (4, 25, 36).

MEA recordings. Extracellular spiking was recorded from cultures plated on planar 64 channel MEAs (Multichannel Systems) recorded between 14-20 DIV in Neurobasal media with B27 and GlutaMax, as described above. Cultured MEAs were covered with custom made MEA rings with gas permeable ethylene-propylene membranes (ALA Scientific Instruments). Synapse software (Tucker-Davis Technologies TDT) was used to monitor activity on a TDT electrophysiological platform consisting of the MEA MZ60 headstage, the PZ2 pre-amplifier and a RZ2 BioAmp Processor. Recordings were band-pass filtered between 200 and 3000Hz and acquired at 25KHz. MEA's were placed in the MZ60 headstage, which was housed in a 5% C02 incubator at 37°C. Drugs were added separately in a sterile hood and then returned to the MEA recording system. MEA spiking activity was analyzed offline with a custom-made Matlab program. The recordings acquired in Synapse software (TDT) were subsequently converted using the subroutine TDT2MAT (TDT) to Matlab files (Mathworks). The custom written Matlab program identified bursts of network spikes using an interspike interval-threshold detection algorithm (37). Spiking activity was labeled as a network burst when it met a user-defined minimum number of spikes (typically 10) occurring across a user-defined minimum number of channels (5-10) within a Time-Window (typically 0.1-0.3 seconds) selected based on the distribution of interspike intervals (typically between the first and 10th consecutive spike throughout the recording, Supplemental Figure 2). This program allowed us to remove silent channels and channels that exhibited high-noise levels. The identified network bursts were then visually inspected to ensure that these parameters accurately identified bursts. The program also computed network burst metrics including burst frequency, overall spike frequency and other characteristics.

Optogenetic control of spiking. For photostimulation experiments neurons were plated on 64-channel planar MEAs and transfected with AAV9-hSynapsin–ChR2(H134R)-eYFP (ChR2) produced by the Emory University Viral Vector Core. All cultures used in ChR2 experiments, including controls, were transfected at 1 DIV. The genomic titer was $1.8x10^{13}$ vg/ml. Virus was diluted 1 to 10,000 in growth medium and this dilution was used for the first medium exchange at DIV 1. Finally, the media containing the virus was washed out after 24 hour incubation. A 3 hour predrug recording was obtained in the TDT program that determined the average MEA-wide firing rate before adding CNQX. This custom written program from TDT then delivered a TTL pulse (50-100ms) that drove a blue light photodiode (465 nm, with a range from 0 to 29.4 mwatts/mm^2, driven by a voltage command of 0-4V) from a custom-made control box that allowed for scaled illumination. The photodiode sat directly below the MEA for activation of the ChR2. This triggered a barrage of spikes resulting in a burst that looked very similar to a naturally occurring burst not in the presence of CNQX. The program measured the MEA-wide spike rate every 10 seconds and if the rate fell below the set value established from the predrug average, an optical stimulation (50-100ms) was delivered triggering a burst which then increased the average firing rate, typically above the set point.

Statistics. Estimation statistics have been used throughout the manuscript. 5000 bootstrap samples were taken; the confidence interval is bias-corrected and accelerated. The *P* value(s) reported are the likelihood(s) of observing the effect size(s), if the null hypothesis of zero difference is true. For each permutation *P* value, 5000 reshuffles of the control and test labels were performed (Moving beyond P values: data analysis with estimation graphics (38).

Acknowledgments

We would like to thank Bill Goolsby who custom built our optogenetic stimulator, and Tucker Davis Technologies for helping us write the Synapse Program that ran the MEA recording/optogenetic stimulation software. We would also like to thank Dr. Gary Bassell for providing us with some of the mice used in culture experiments.

\

References

1. N. W. Tien, D. Kerschensteiner, Homeostatic plasticity in neural development. *Neural Dev* **13**, 9 (2018).
2. G. G. Turrigiano, K. R. Leslie, N. S. Desai, L. C. Rutherford, S. B. Nelson, Activity-dependent scaling of quantal amplitude in neocortical neurons. *Nature* **391**, 892-896. (1998).
3. G. Turrigiano, Homeostatic synaptic plasticity: local and global mechanisms for stabilizing neuronal function. *Cold Spring Harb Perspect Biol* **4**, a005736 (2012).
4. A. L. Hanes *et al.*, Divergent Synaptic Scaling of Miniature EPSCs following Activity Blockade in Dissociated Neuronal Cultures. *J Neurosci* **40**, 4090-4102 (2020).
5. G. Wang, J. Zhong, D. Guttieres, H. Y. Man, Non-scaling regulation of AMPA receptors in homeostatic synaptic plasticity. *Neuropharmacology* **158**, 107700 (2019).
6. Q. Hou, D. Zhang, L. Jarzylo, R. L. Huganir, H. Y. Man, Homeostatic regulation of AMPA receptor expression at single hippocampal synapses. *Proc Natl Acad Sci U S A* **105**, 775-780 (2008).
7. M. A. Sutton *et al.*, Miniature neurotransmission stabilizes synaptic function via tonic suppression of local dendritic protein synthesis. *Cell* **125**, 785-799 (2006).
8. J. C. Beique, Y. Na, D. Kuhl, P. F. Worley, R. L. Huganir, Arc-dependent synapse-specific homeostatic plasticity. *Proc Natl Acad Sci U S A* **108**, 816-821 (2011).
9. K. E. Deeg, C. D. Aizenman, Sensory modality-specific homeostatic plasticity in the developing optic tectum. *Nat Neurosci* **14**, 548-550 (2011).
10. K. Ibata, Q. Sun, G. G. Turrigiano, Rapid synaptic scaling induced by changes in postsynaptic firing. *Neuron* **57**, 819-826 (2008).
11. J. Burrone, M. O'Byrne, V. N. Murthy, Multiple forms of synaptic plasticity triggered by selective suppression of activity in individual neurons. *Nature* **420**, 414-418 (2002).
12. M. F. Fong, J. P. Newman, S. M. Potter, P. Wenner, Upward synaptic scaling is dependent on neurotransmission rather than spiking. *Nat Commun* **6**, 6339 (2015).
13. M. A. Garcia-Bereguiain, C. Gonzalez-Islas, C. Lindsly, P. Wenner, Spontaneous Release Regulates Synaptic Scaling in the Embryonic Spinal Network In Vivo. *J Neurosci* **36**, 7268-7282 (2016).
14. V. Kilman, M. C. van Rossum, G. G. Turrigiano, Activity deprivation reduces miniature IPSC amplitude by decreasing the number of postsynaptic GABA(A) receptors clustered at neocortical synapses. *J Neurosci* **22**, 1328-1337. (2002).
15. C. C. Swanwick, N. R. Murthy, J. Kapur, Activity-dependent scaling of GABAergic synapse strength is regulated by brain-derived neurotrophic factor. *Mol Cell Neurosci* **31**, 481-492 (2006).

16. K. N. Hartman, S. K. Pal, J. Burrone, V. N. Murthy, Activity-dependent regulation of inhibitory synaptic transmission in hippocampal neurons. *Nat Neurosci* **9**, 642-649 (2006).
17. Y. R. Peng *et al.*, Postsynaptic spiking homeostatically induces cell-autonomous regulation of inhibitory inputs via retrograde signaling. *J Neurosci* **30**, 16220-16231 (2010).
18. P. Wenner, Mechanisms of GABAergic homeostatic plasticity. *Neural Plast* **2011**, 489470 (2011).
19. A. Joseph, G. G. Turrigiano, All for One But Not One for All: Excitatory Synaptic Scaling and Intrinsic Excitability Are Coregulated by CaMKIV, Whereas Inhibitory Synaptic Scaling Is Under Independent Control. *J Neurosci* **37**, 6778-6785 (2017).
20. M. A. Gainey, J. W. Aman, D. E. Feldman, Rapid Disinhibition by Adjustment of PV Intrinsic Excitability during Whisker Map Plasticity in Mouse S1. *J Neurosci* **38**, 4749-4761 (2018).
21. L. Li, M. A. Gainey, J. E. Goldbeck, D. E. Feldman, Rapid homeostasis by disinhibition during whisker map plasticity. *Proc Natl Acad Sci U S A* **111**, 1616-1621 (2014).
22. K. B. Hengen, M. E. Lambo, S. D. Van Hooser, D. B. Katz, G. G. Turrigiano, Firing rate homeostasis in visual cortex of freely behaving rodents. *Neuron* **80**, 335-342 (2013).
23. S. J. Barnes *et al.*, Subnetwork-Specific Homeostatic Plasticity in Mouse Visual Cortex In Vivo. *Neuron* **86**, 1290-1303 (2015).
24. S. J. Kuhlman *et al.*, A disinhibitory microcircuit initiates critical-period plasticity in the visual cortex. *Nature* **501**, 543-546 (2013).
25. A. G. Koesters, M. M. Rich, K. L. Engisch, Diverging from the Norm: Reevaluating What Miniature Excitatory Postsynaptic Currents Tell Us about Homeostatic Synaptic Plasticity. *Neuroscientist* 10.1177/10738584221112336, 10738584221112336 (2022).
26. D. A. Wagenaar, J. Pine, S. M. Potter, An extremely rich repertoire of bursting patterns during the development of cortical cultures. *BMC Neurosci* **7**, 11 (2006).
27. C. P. Goold, R. A. Nicoll, Single-cell optogenetic excitation drives homeostatic synaptic depression. *Neuron* **68**, 512-528 (2010).
28. K. G. Pratt, C. D. Aizenman, Homeostatic regulation of intrinsic excitability and synaptic transmission in a developing visual circuit. *J Neurosci* **27**, 8268-8277 (2007).
29. J. Aoto, C. I. Nam, M. M. Poon, P. Ting, L. Chen, Synaptic signaling by all-trans retinoic acid in homeostatic synaptic plasticity. *Neuron* **60**, 308-320 (2008).
30. C. Gonzalez-Islas, P. Bulow, P. Wenner, Regulation of synaptic scaling by action potential-independent miniature neurotransmission. *J Neurosci Res* **96**, 348-353 (2018).

31. M. A. Gainey, D. E. Feldman, Multiple shared mechanisms for homeostatic plasticity in rodent somatosensory and visual cortex. *Philos Trans R Soc Lond B Biol Sci* **372** (2017).
32. A. Ribic, Stability in the Face of Change: Lifelong Experience-Dependent Plasticity in the Sensory Cortex. *Front Cell Neurosci* **14**, 76 (2020).
33. E. Fino, A. M. Packer, R. Yuste, The logic of inhibitory connectivity in the neocortex. *Neuroscientist* **19**, 228-237 (2013).
34. A. M. Packer, R. Yuste, Dense, unspecific connectivity of neocortical parvalbumin-positive interneurons: a canonical microcircuit for inhibition? *J Neurosci* **31**, 13260-13271 (2011).
35. L. C. Rutherford, A. DeWan, H. M. Lauer, G. G. Turrigiano, Brain-derived neurotrophic factor mediates the activity-dependent regulation of inhibition in neocortical cultures. *J Neurosci* **17**, 4527-4535. (1997).
36. D. Pekala, P. Wenner, The uniform and non-uniform nature of slow and rapid scaling in embryonic motoneurons. *J Neurosci* 10.1523/JNEUROSCI.0899-21.2021 (2021).
37. D. J. Bakkum *et al.*, Parameters for burst detection. *Front Comput Neurosci* **7**, 193 (2013).
38. J. Ho, T. Tumkaya, S. Aryal, H. Choi, A. Claridge-Chang, Moving beyond P values: data analysis with estimation graphics. *Nat Methods* **16**, 565-566 (2019).

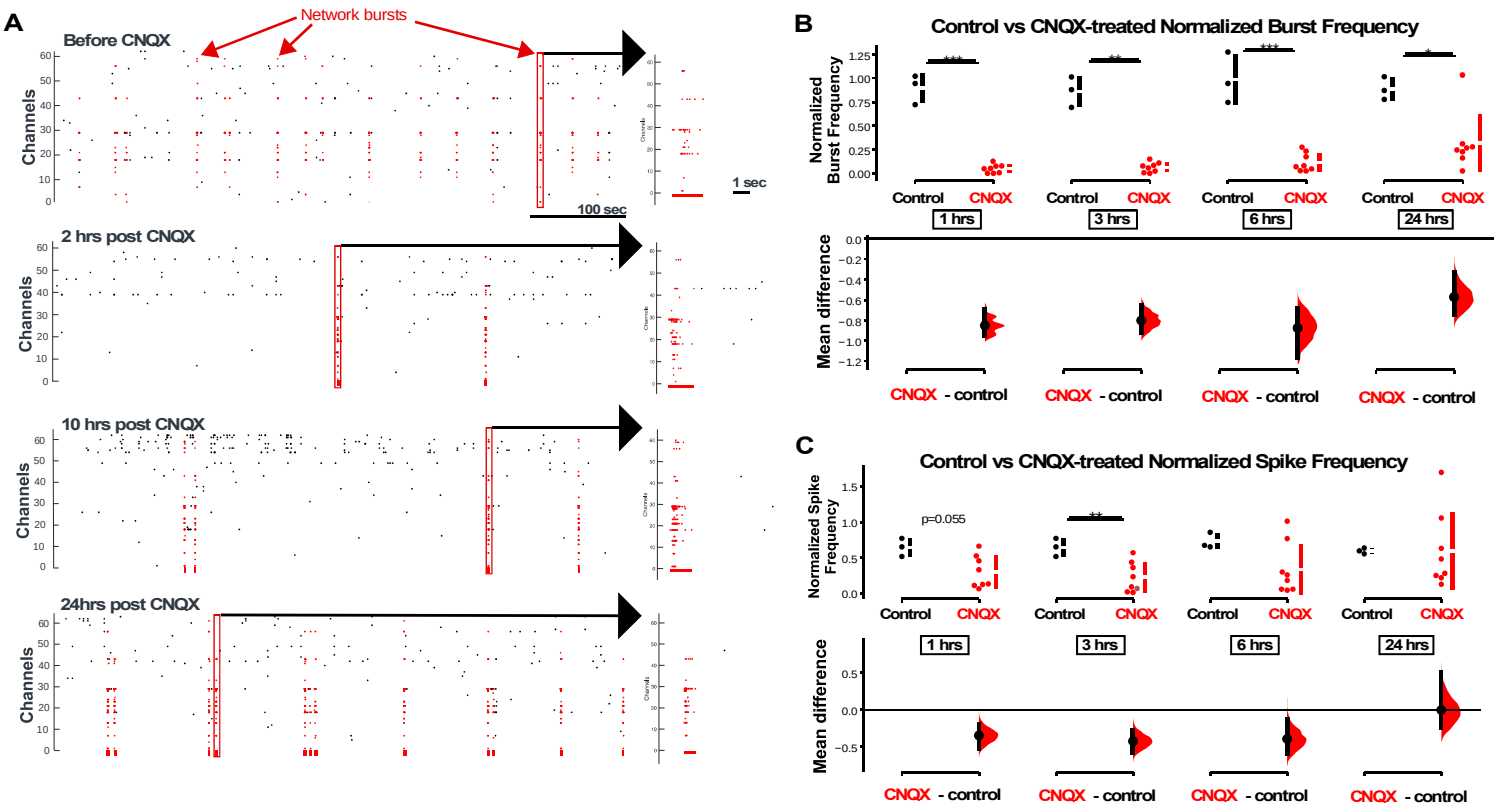

Figure 1. AMPAergic blockade reduces burst frequency and overall spike rate. A) Network bursts can be identified by detected spikes (red dots) time-locked in multiple channels of the MEA (Y axis). One burst (highlighted in red rectangle) is expanded in time and shown in the raster plot on the right. This is illustrated before CNQX (top) and then repeated below at 2hrs, 10 hrs, and 24 hrs following the addition of CNQX. B) The normalized burst rate is shown in control cultures and following application of CNQX for 24 hrs. C) The normalized overall spike rate is shown in control cultures and following CNQX addition over 24 hrs. The mean differences at different time points are compared to control and displayed in Cumming estimation plots. Significant differences denoted by * $p \leq 0.05$, ** $p \leq 0.01$, *** $p \leq 0.001$. Recordings from single cultures (filled circles), where mean values (represented by the gap in the vertical bar) and SD (vertical bars) are plotted on the upper panels. Mean differences between control and treated groups are plotted on the bottom panel, as a bootstrap sampling distribution (mean difference is represented by a filled circles and the 95% CIs are depicted by vertical error bars).

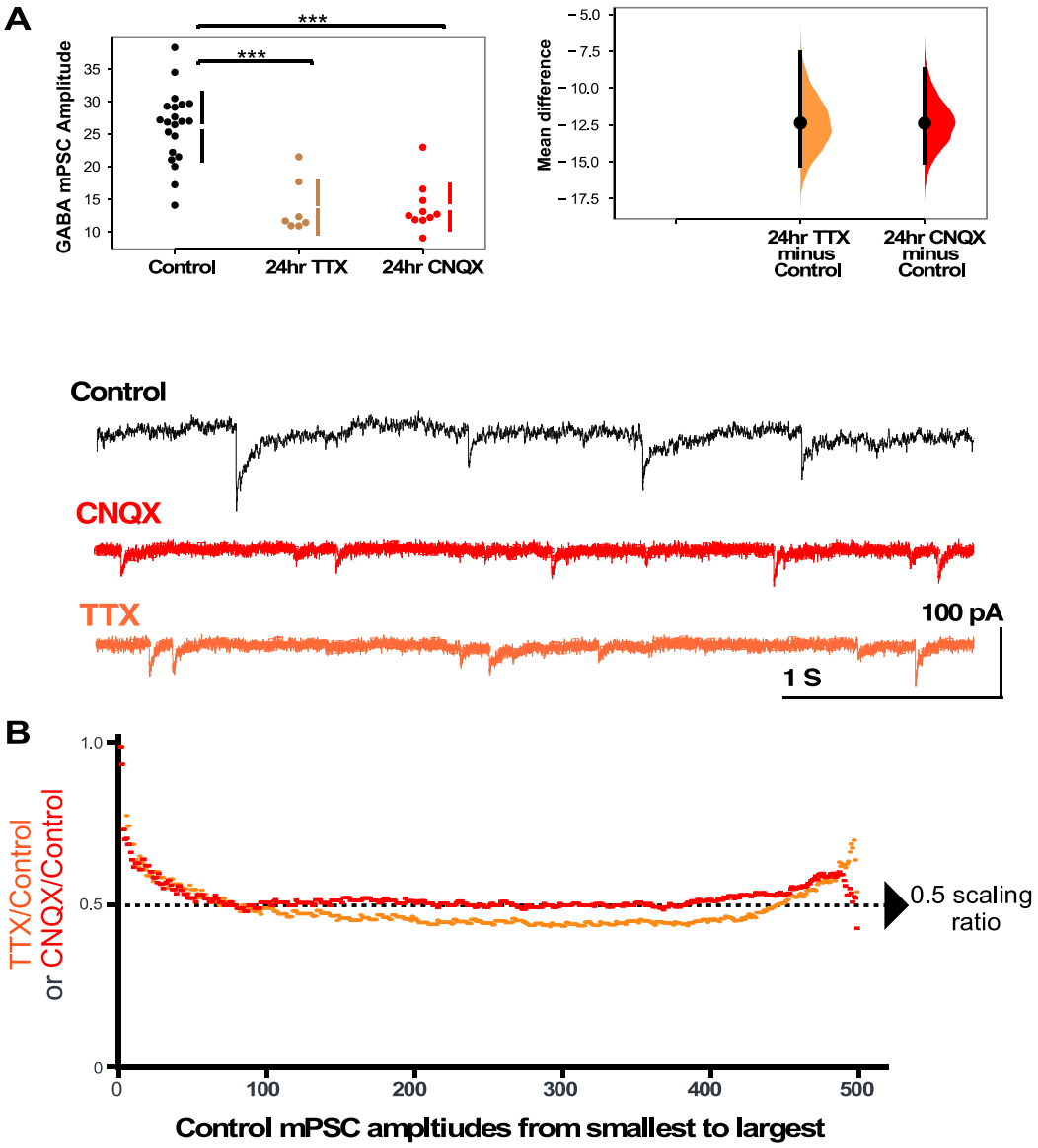

Figure 2. Both activity and AMPAR blockade cause a reduction in mIPSC amplitudes that appear to scale down. A) CNQX and TTX produce a reduction in average amplitude of mIPSCs as shown in the scatter plot. The mean differences are compared to control and displayed in Cumming estimation plots. Significant differences denoted by *** $p \leq 0.001$. GABAergic mPSC amplitudes from single neurons (filled circles), where mean values (represented by the gap in the vertical bar) and SD (vertical bars) are plotted on the panels to the left. Mean differences between control and treated groups are plotted on the panel to the right, as a bootstrap sampling distribution (mean difference is represented by a filled circles and the 95% CIs are depicted by vertical error bars). Example traces showing mIPSCs are shown below. B) Scaling ratio plots show the relationship of mIPSC amplitudes from treated cultures compared to untreated cultures. All recordings taken from cultured neurons plated on coverslips, not MEAs.

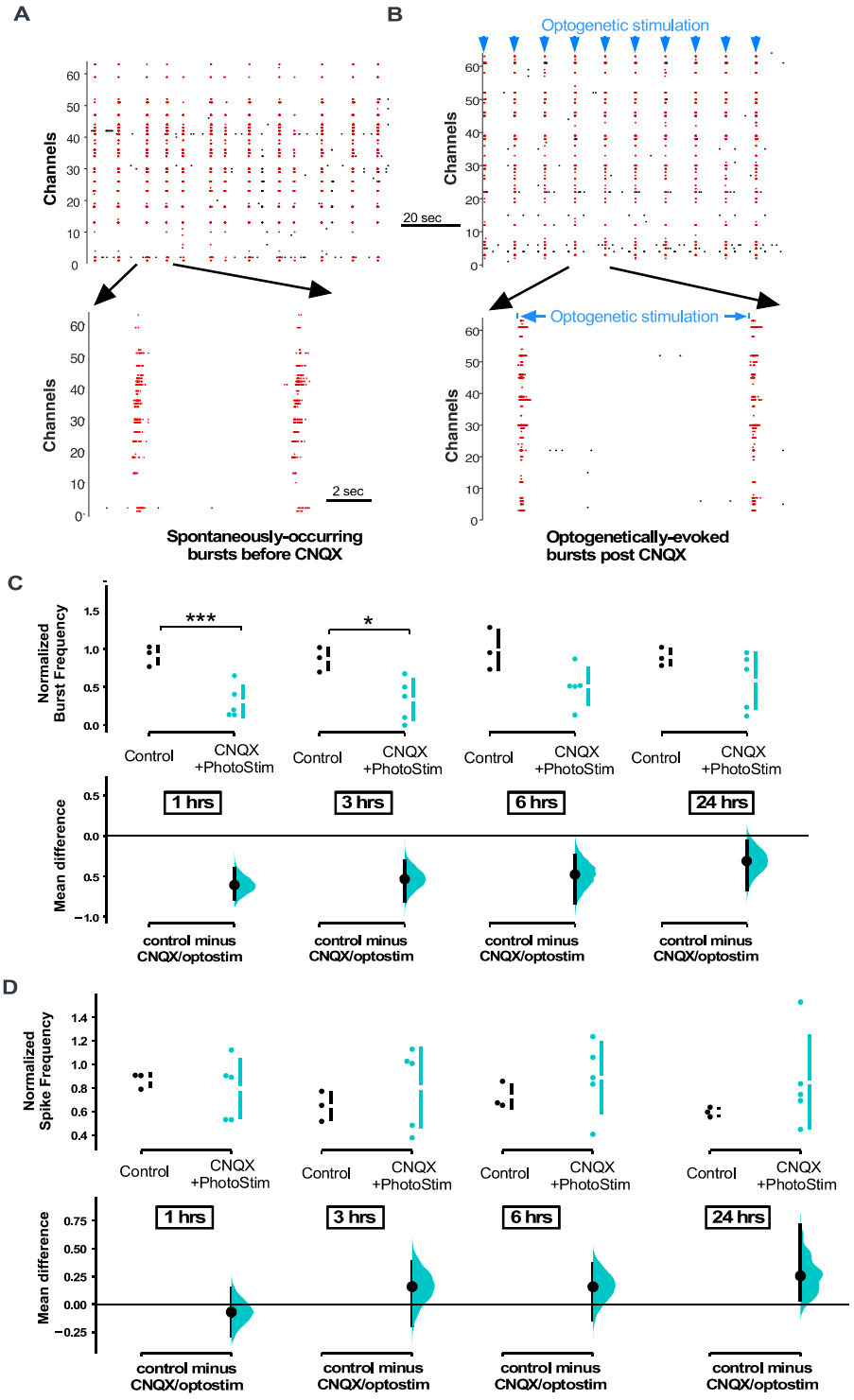

Figure 3. MEA recordings show that optogenetic stimulation restores spiking activity in cultures treated with CNQX. A) Spontaneously-occuring bursts of spiking are identified (synchronous spikes/red dots). Expanded version of raster plot highlighting 2 bursts is shown below. B) Same as in A, but after CNQX was added to the bath and bursts were now triggered by optogenetic stimulation (blue line shows duration of optogenetic stimulation). C-D) Average burst rate (C) or spike rate (D) is compared for CNQX-treated cultures with optogenetic stimulation and control unstimulated cultures at 1hr, 3hrs, 6hrs, and 24hrs after addition of CNQX or vehicle (same control data presented in Figure 4). The mean differences at different time points are compared to control and displayed in Cumming estimation plots. Significant differences denoted by * $p \leq 0.05$, *** $p \leq 0.001$. Recordings from single cultures (filled circles), where mean values (represented by the gap in the vertical bar) and SD (vertical bars) are plotted on the upper panels. Mean differences between control and treated groups are plotted on the bottom panel, as a bootstrap sampling distribution (mean difference is represented by a filled circles and the 95% CIs are depicted by vertical error bars).

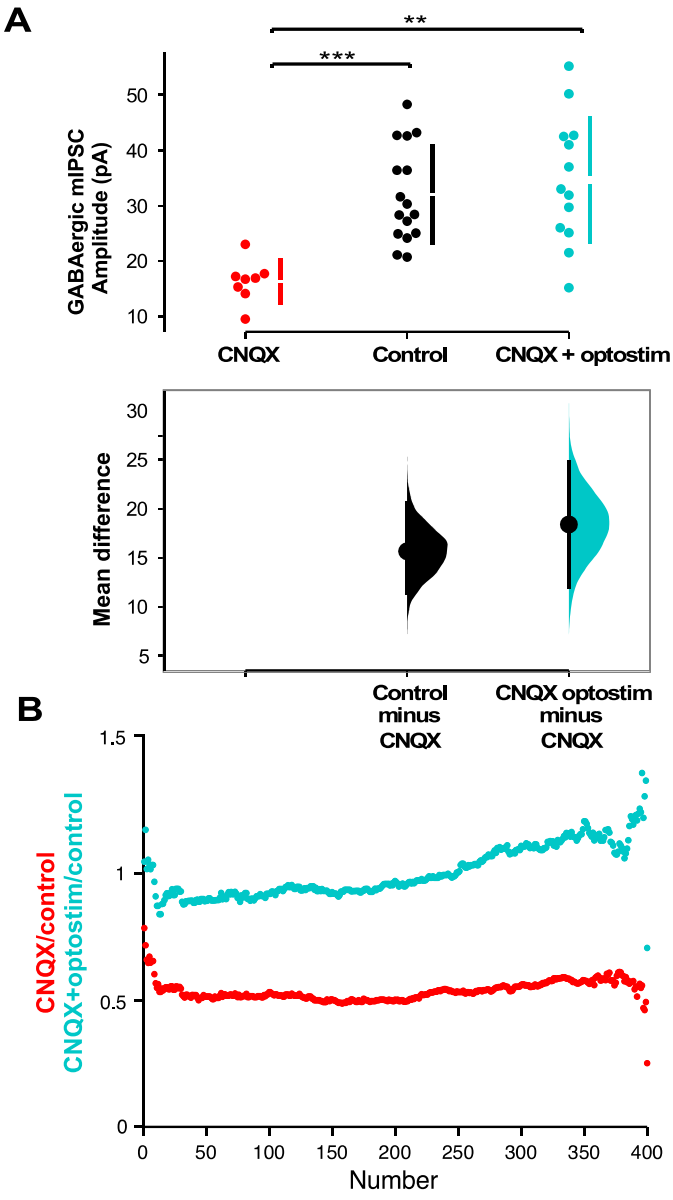

Figure 4. Optogenetic restoration of spiking activity in the presence of AMPAR blockade prevents GABAergic downscaling observed in CNQX alone. A) Scatter plot shows AMPAR blockade triggers a reduction in mIPSC amplitude compared to controls that is prevented when combined with optogenetic stimulation (optostim). The mean differences are compared to control and displayed in Cumming estimation plots. Significant differences denoted by ** $p \leq 0.01$, *** $p \leq 0.001$. GABAergic mPSC amplitudes from single neurons (filled circles), where mean values (represented by the gap in the vertical bar) and SD (vertical bars) are plotted on the upper panels. Mean differences between control and treated groups are plotted on the bottom panel, as a bootstrap sampling distribution (mean difference is represented by a filled circles and the 95% CIs are depicted by vertical error bars). B) Scaling ratio plots show largely multiplicative relationships to control values for both CNQX and CNQX + photostimulation treatments. Cultured neurons for these recordings were obtained from cells plated on MEAs (control, CNQX, and CNQX+optostim).

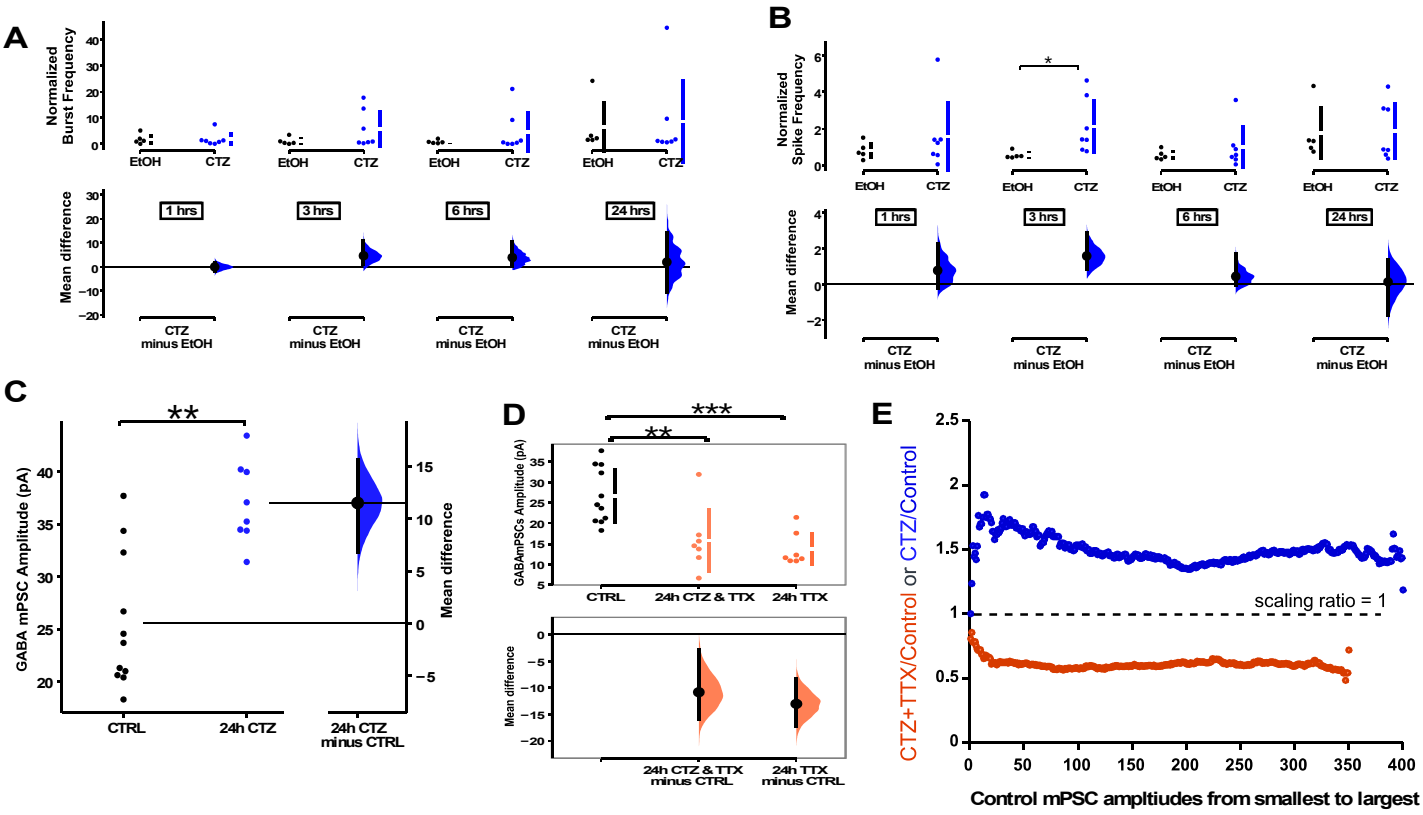

Figure 5. GABAergic upscaling was also triggered by changes in spiking activity rather than AMPAR activation. MEA recordigns show that CTZ trended toward increases of both burst rate (A) and overall spike frequency (B) during the 24 hr application, and achieved significance at the 3 hr timepoint for spike frequency. C) CTZ treatment (dissolved in 1:1000 dilution of ethanol (EtOH)) led to an increase in mIPSC amplitude compared to control cultures (equivalent volume of 1:1000 ethanol solution). D) CTZ combined with TTX (in 1:1000 ethanol) produced a reduction of mIPSC amplitude compared to controls (that was no different than TTX alone). The mean differences at different time points or conditions are compared to control and displayed in Cumming estimation plots. Significant differences denoted by * $p \leq 0.05$, ** $p \leq 0.01$, *** $p \leq 0.001$. Recordings from single cultures (filled circles), where mean values (represented by the gap in the vertical bar) and SD (vertical bars) are plotted on the upper panels. Mean differences between control and treated groups are plotted on the bottom panel, as a bootstrap sampling distribution (mean difference is represented by a filled circles and the 95% CIs are depicted by vertical error bars). E) Scaling ratios show that both CTZ-induced increases and CTZ+TTX -induced decreases were multiplicative. All mIPSC amplitudes recorded from cultures plated on coverslips, not MEAs.

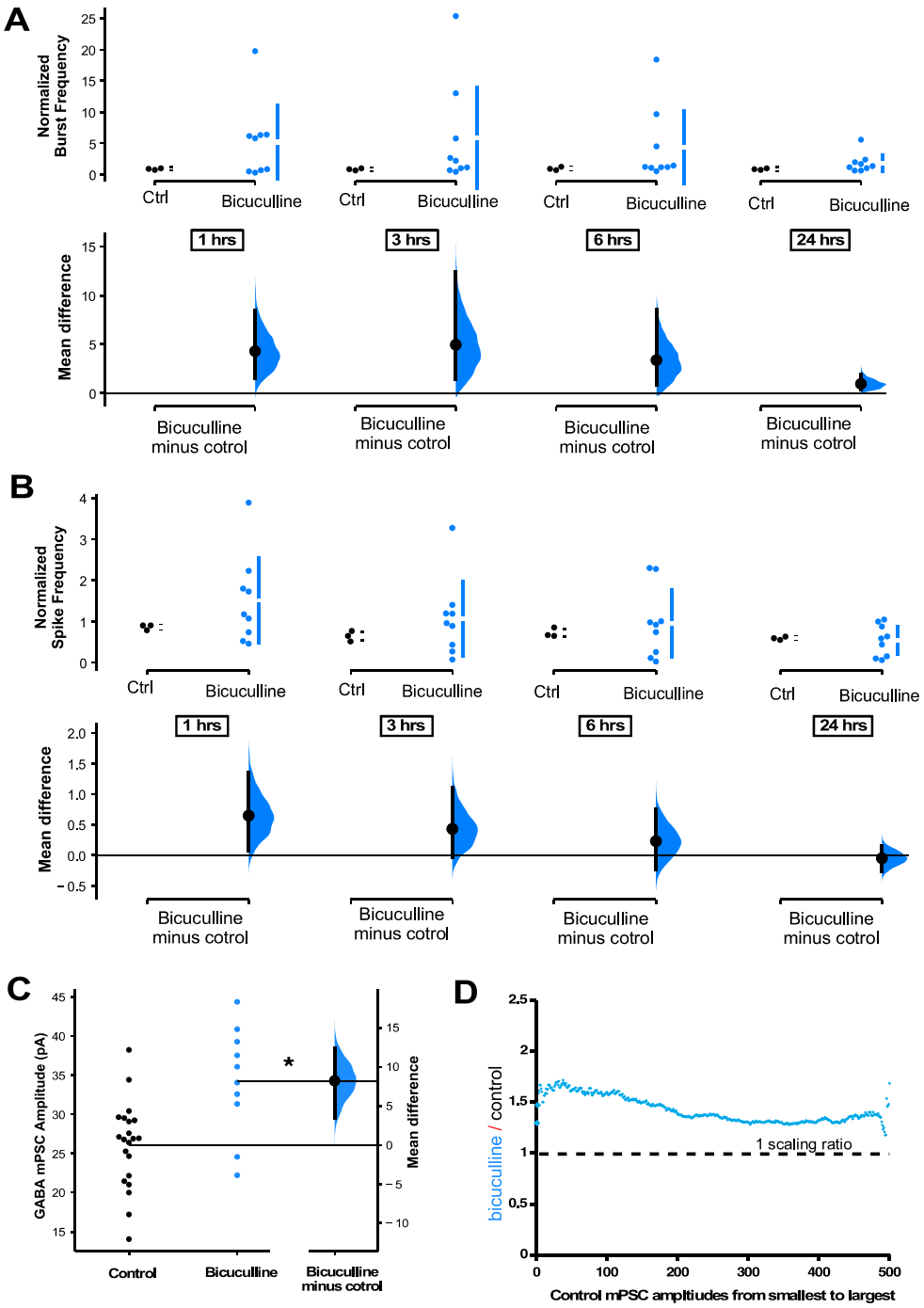

Figure 6. GABAergic upscaling is triggered by increased spiking activity rather than reduced GABAR activation. Bicuculline-treated cultures (24hrs) plated on MEA's trended upward in burst frequency (A) and overall spike frequency (B). Recordings from single cultures (filled circles), where mean values (represented by the gap in the vertical bar) and SD (vertical bars) are plotted on the upper panels. C) Bicuculline treatment (24hrs) produced an increase in mIPSC amplitudes. The mean difference is compared to control and displayed in Cumming estimation plots. Significant difference denoted by * $p \leq 0.05$. Recordings from single neurons (filled circles), and mean values (represented by the horizontal line). Control and treated group is plotted, as a bootstrap sampling distribution (mean difference is represented by a filled circles and the 95% CI is depicted by vertical error bar). D) Ratio plots for bicuculline-induced increase in mIPSCs exhibits a multiplicative profile. All mIPSC amplitudes recorded from cultures plated on coverslips, not MEAs.

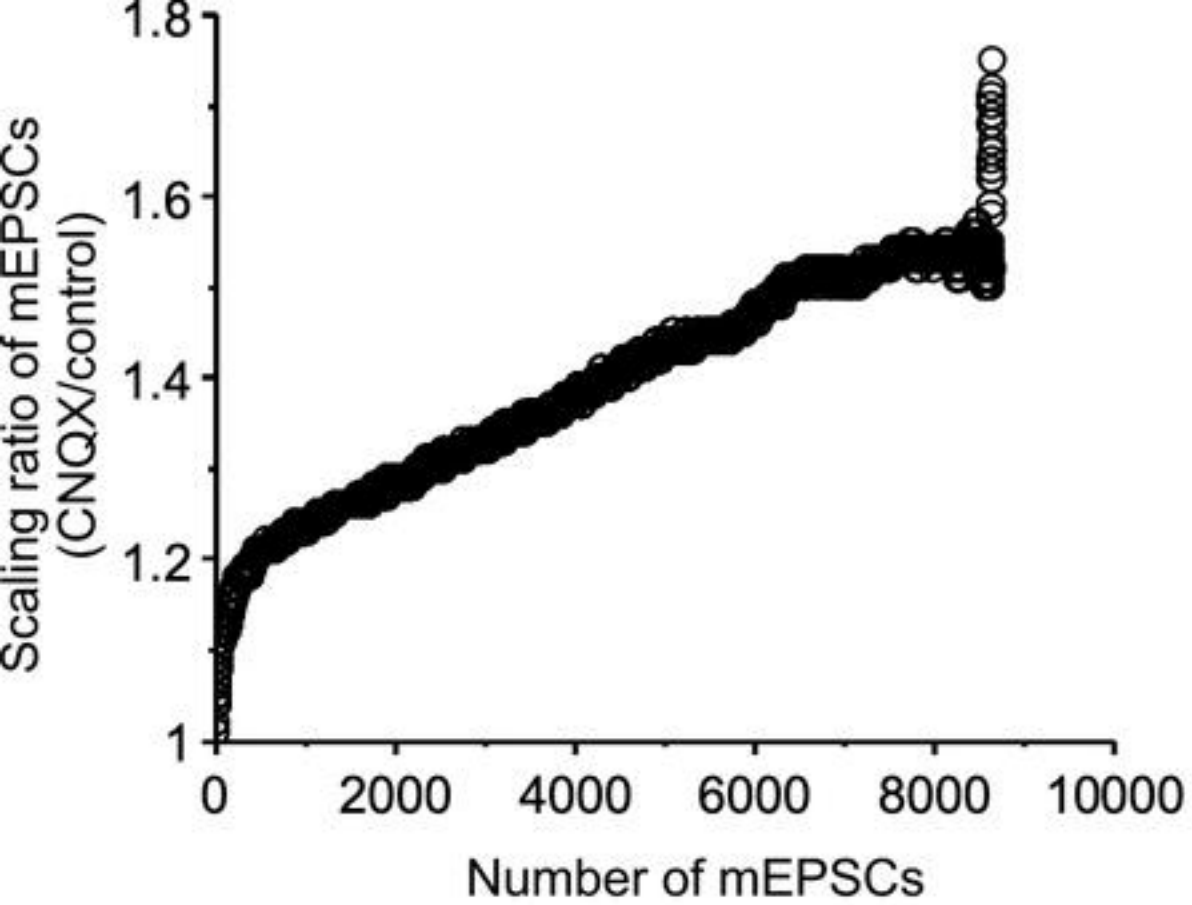

Supplemental Figure 1. AMPAR block triggered non-uniform AMPAergic scaling. Scaling ratio plot shows the ratio of rank ordered mEPSC amplitudes from CNQX-treated cultures (n=95 cells, 91mEPSCs/cell) divided by those from untreated cultures (n=91 cells, 95 mEPSCs/cell). The X axis represents the rank ordered number of mEPSCs (from smallest to largest).

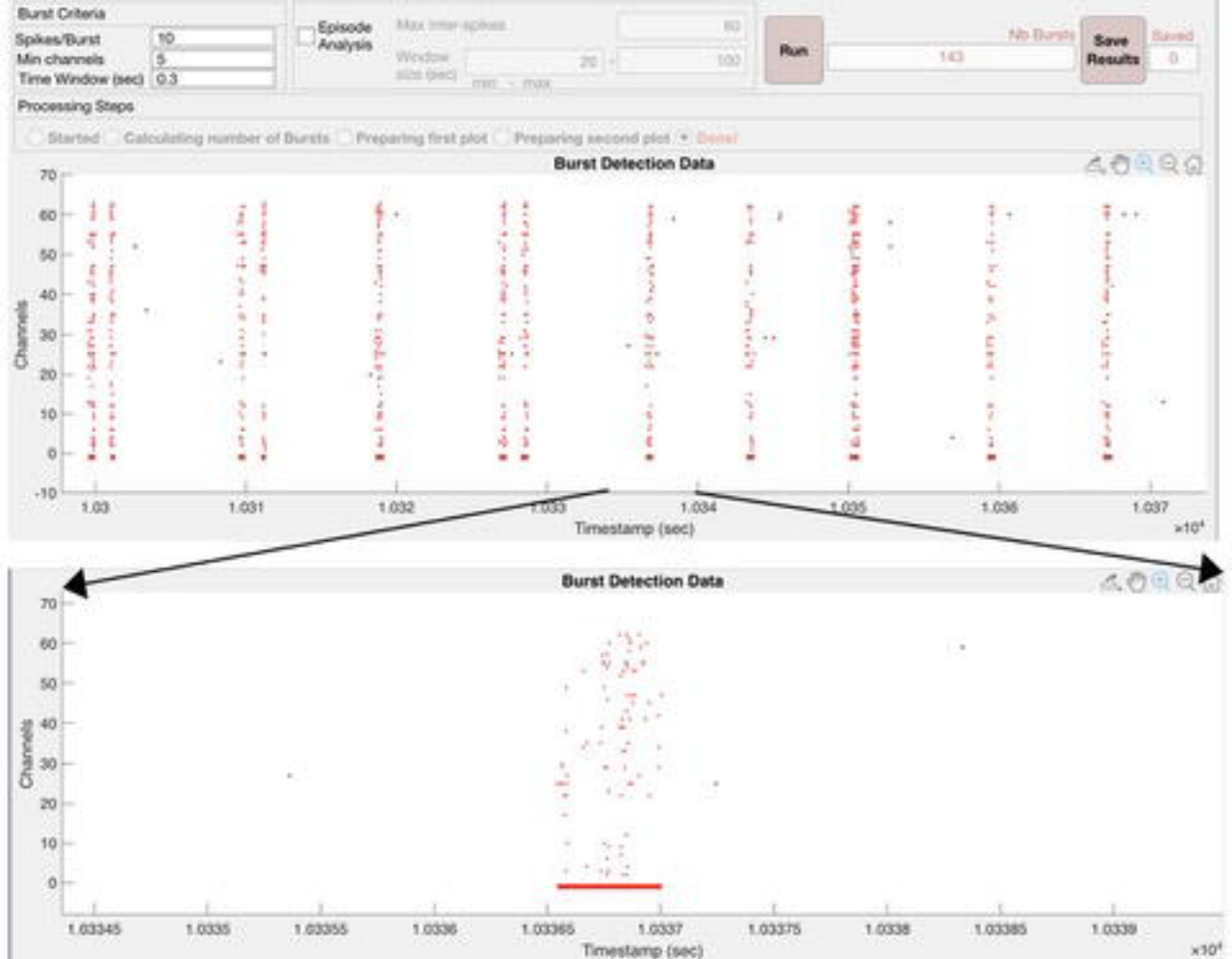

Supplemental Figure 2. Custom written Matlab program identifies bursts in cortical cultures plated on MEA's by choosing the minimum number of spikes per burst (Spikes/Burst) across a minimum number of channels contributing to a burst (Min channels) within a maximum Time Window. Upper image shows the identification of bursts in red across 64 channels as a raster plot where each dot represents one spike detected on the MEA. The program then examines various parameters which were then exported to an excel spreadsheet for analysis. Burst identitiy and duration are shown as a red line positioned below the raster plot. A single burst is expanded and plotted below the upper image.

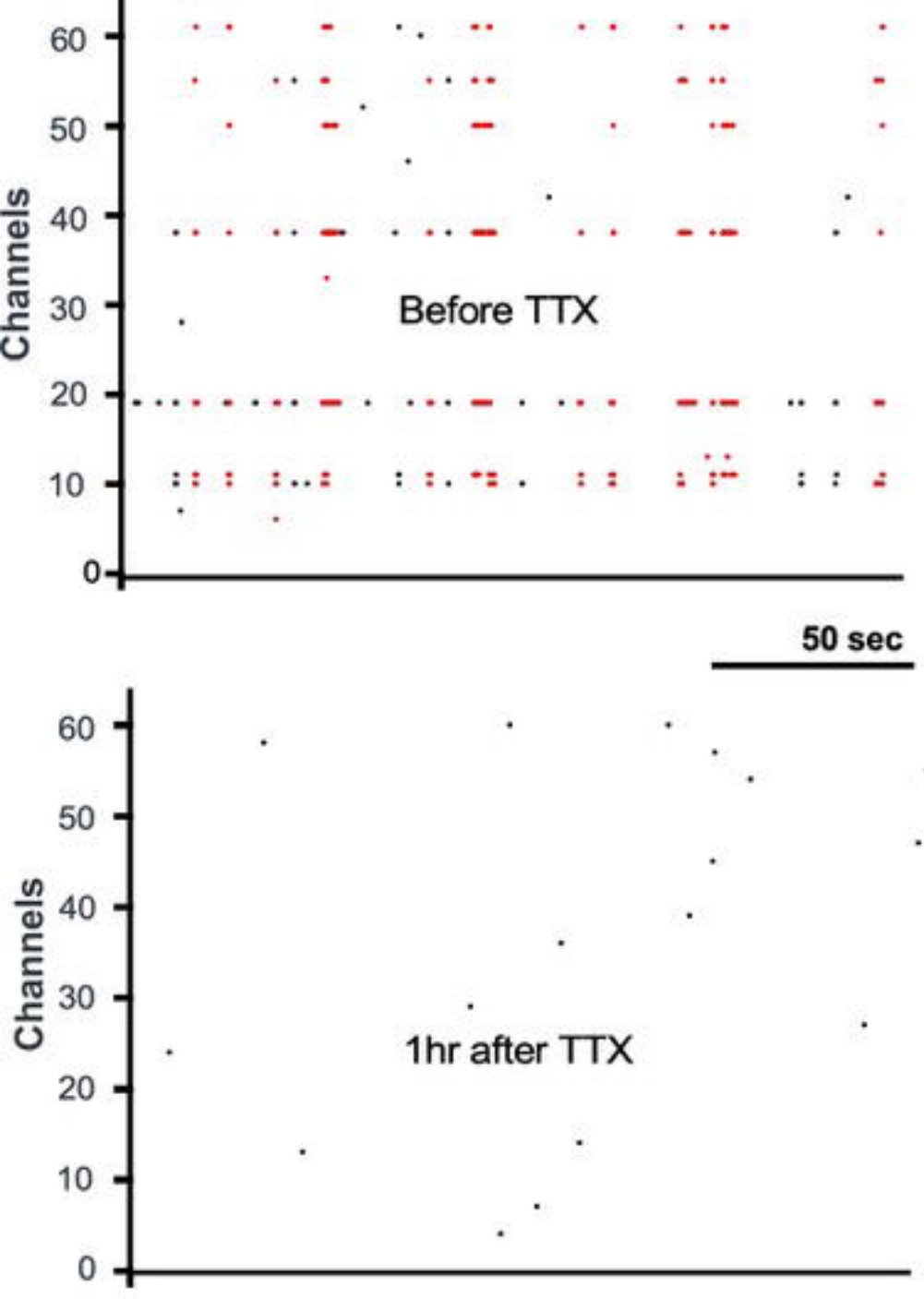

Supplemental FIgure 3. Rasterplot of cortical culture plated on MEA demonstrating network bursting (red dots, upper plot). Bursts were then abolished after addition of TTX (1μM) to the culture; a small number of spike detections remain, however these are likey to be noise that crosses the detection threshold.

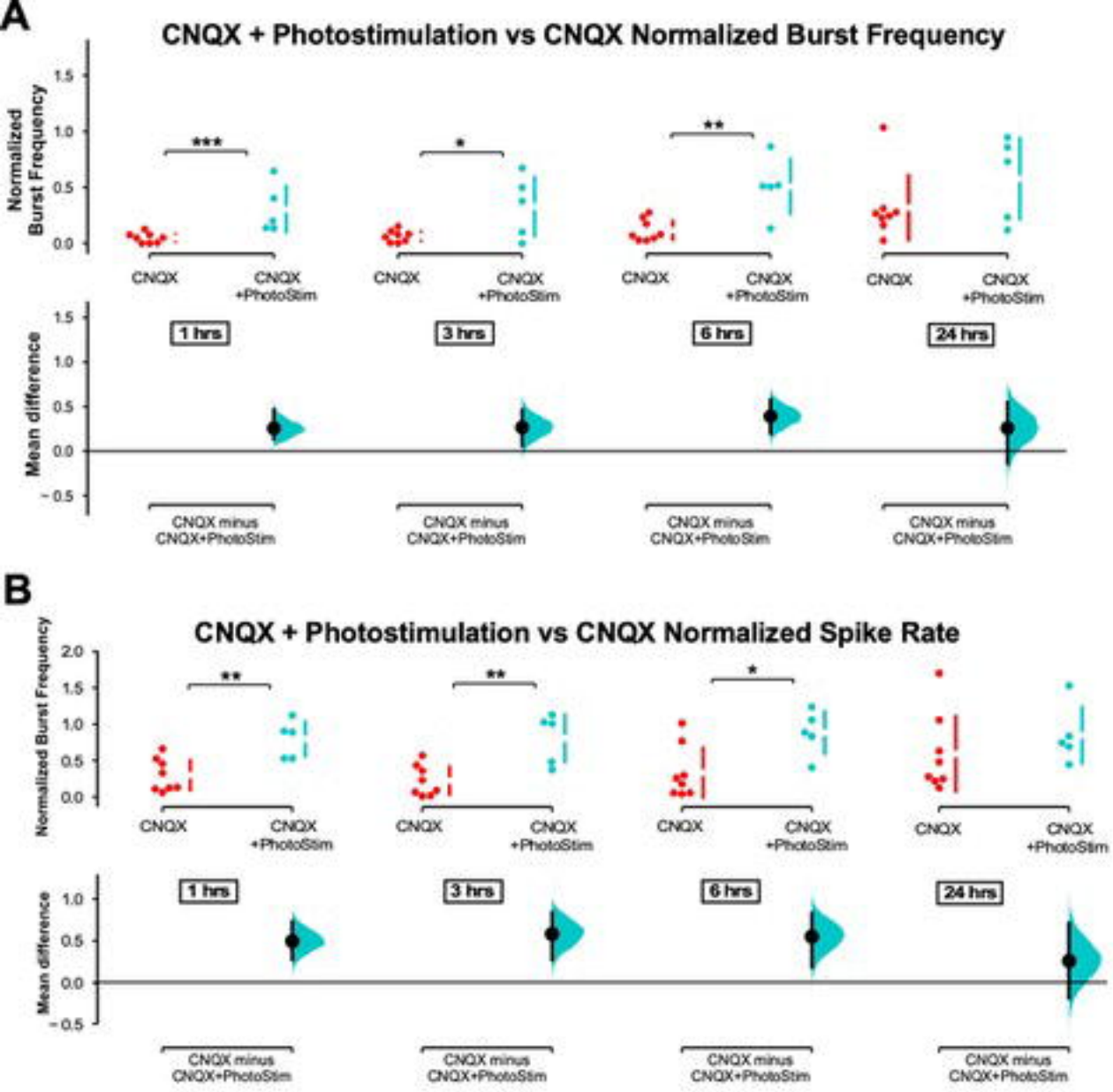

Supplemental Figure 4. MEA recordigns show optostim + CNQX increases burst frequency and spike frequency compared to CNQX alone. A-B) The average Burst rate (A) or spike frequency (B) is shown in cultures following CNQX + photostim or just CNQX over 24 hrs. The mean differences at different time points are compared to control and displayed in Cumming estimation plots. Significant differences denoted by * $p \leq 0.05$, ** $p \leq 0.01$, *** $p \leq 0.001$. Recordings from single cultures (filled circles), where mean values (represented by the gap in the vertical bar) and SD (vertical bars) are plotted on the upper panels. Mean differences between control and treated groups are plotted on the bottom panel, as a bootstrap sampling distribution (mean difference is represented by a filled circles and the 95% CIs are depicted by vertical error bars).